EUROFUSION WPMAT-PR(15) 14579

F Granberg et al.

EFFECT OF OBSTACLE NANOSTRUCTURE ON THE MOVEMENT OF EDGE DISLOCATIONS IN BCC FE

Preprint of Paper to be submitted for publication in
Nuclear Materials and Energy

This work has been carried out within the framework of the EUROfusion Consortium and has received funding from the Euratom research and training programme 2014-2018 under grant agreement No 633053. The views and opinions expressed herein do not necessarily reflect those of the European Commission.

- 00 (2015) 1–10

EFFECT OF OBSTACLE NANOSTRUCTURE ON THE MOVEMENT OF EDGE DISLOCATIONS IN BCC FE

F. Granberg[a,*], K. Nordlund[a]

[a]*Department of Physics, P.O. Box 43, FIN-00014 University of Helsinki, Finland*

Abstract

In this study we investigate how different obstacle nanostructures affect the edge dislocation movement in an iron matrix by Molecular Dynamics simulations. We investigate the effect of temperature, size of the obstacle and composition of the obstacle on the unpinning mechanism for dislocations. Beside the mechanism present when the dislocation bypasses the different obstacles we have determined the unpinning stress for all obstacles. We investigated nine different obstacles of three different sizes at five different temperatures. All simulations were performed in the same system setup, with the same parameters, to ensure comparable results. The results show that different kinds of obstacles will have different mechanisms, even the size can in certain cases change the mechanism. We found that temperature will not change the mechanism, but it will change the features of the unpinning mechanism, like speed up the processes, resulting in lower unpinning stresses. We also saw that obstacles with the same size and same unpinning mechanism will result in similar unpinning stresses. For the obstacles with different mechanisms there was a noticable difference in the needed unpinning stress between same sized obstacles.

Keywords:
dislocation, molecular dynamics, precipitate

1. Introduction

In demanding environments, like nuclear power plants, the mechanical properties of the structural materials is crucial to know. These demanding environments can be due to the constant radiation present or the loading and unloading of the structural materials in constructions. Most structural parts are made from some variety of steel, which has a complex nanostructure of precipitates, grains, inclusions and alloying elements. The complex nanostructure is the key to the good mechanical and other properties of steels, and therefore further improvements by informed choices can probably be made. The mechanical properties of metals are determined by the movement of dislocations and the interaction of the dislocations with the different features. Therefore it is important to know how the dislocations are interacting with the different features, to be able to predict the properties of the material.

The dislocations are usually pinned by the obstacles and there is a certain stress at which the dislocation can unpin from the obstacle. The unpinning stress is one of the parameters important to know for the different features in the material. Another important parameter is the mechanism that is present when the dislocation is unpinning from the obstacle. The unpinning stress will determine the immediate strength of the obstacle. Different mechanisms will on the other hand determine the evolution of both the dislcoation and the obstacles, some mechanisms will destroy the obstacle and therefore make the material softer and some mechanisms will make the material stronger, but also more

*Corresponding author.
Email address: fredric.granberg@helsinki.fi (F. Granberg)

brittle. Both of these can have detrimental consequences, if the phenomena is not known or expected. These two parameters, which are related to each other, are a result of the interaction of dislocations with obstacles on an atomic scale, which is why Molecular Dynamics simulations are well suited to study both of these. These results can be used as parameters in or to parametrize higher scale models, such as Dislocation Dynamics. The unpinning stress can be used to adjust the strength of obstacles and the obstacle can be adjusted so that the right mechanism is present. The different mechanism and setups to achieve these in Dislocation Dynamics have been studied previously [1, 2, 3]. In this Article we focus on what unpinning mechanism is present for different kinds of obstacles. How different circumstances will change the unpinning mechanism as well as the unpinning strength and the consequences of this are also investigated.

In this Article we have investigated and compared nine different obstacles in pure iron, to determine both the unpinning stress and the unpinning mechanism for edge dislocations, by means of classical Molecular Dynamics simulations. The effect of obstacle size and temperature is also investigated on both of these properties. All simulations are conducted in the same system setup and the same input parameters are used to ensure comparability between the results of the different obstacles.

2. Methods

The simulations were performed with the classical Molecular Dynamics code PARCAS [4, 5], with an interatomic potential, describing Fe, Cr and C interactions, by Henriksson *et al.* [6]. The simulation setup was according to the setup described in Ref. 7, by Osetsky and Bacon. The x-, y- and z-axis were oriented along the [111], [$\bar{1}\bar{1}$2] and [1$\bar{1}$0]-directions, respectively, in the BCC structured simulation cell. An edge dislocation with the Burgers's vector $\mathbf{b} = 1/2[111]$ was generated in the $x - y$ slip plane. The dislocation was generated by placing N layers in the top half and $N - 1$ layers in the bottom half, and then compressing and extending the halfs by the Burger's vector per two to match the two halfs. This will introduce a perfect edge-dislocation in the middle of the cell. A few layers of atoms were fixed in the top- and the bottom-part of the z-direction, and a Berendsen type themostat was applied on a few layers of atoms above the fixed atoms at the bottom.

The fixed layers at the top were moved by a constant strain rate of 5×10^7 s^{-1} in the x-direction, to induce a glide force on the edge dislocation. A schematic illustration of the system setup can be seen in Fig. 1, where the gray boxes are the fixed regions and the gray plane the slip plane where the dislocation is moving in. The pristine box with the pre-existing edge dislocation contained 542,700 atoms, which was the starting point for the generation of the simulation cells with the different obstacles. The box was 101×3, 30×6 and 30×2 atomic planes in x-, y- and z-directions, respectively. This resulted in a box size of $25 \times 21 \times 12$ nm^3. Periodic boundary conditions were applied in the x- and y-directions. The length of the dislocations between the obstacles was 21 nm $- d_p$, where d_p is the diameter of the obstacle. The same box size and strain rate have been used in previous studies, and some of the results are taken from them, Refs. 8 and 9.

In the investigation of the size effect we used three different sizes, 1 nm, 2 nm and 4 nm and the temperatures studied were 300 K, 450 K, 600 K, 750 K and 900 K. The used potential and strain rate showed a temperature dependent flow stress, this value have been subtracted from the numerical results, to get the contribution of only the obstacle. The flowstress was 90 MPa, 85 MPa, 80 MPa, 75 MPa and 70 MPa for the increasing temperature. To visualize the interaction of the dislocation with the obstacle the program OVITO [10], and the Adaptive Common Neighbor Analyzis implemented in the program, were used. The evolution of all obstacles were investigated during several interaction with the same dislocations, *e.g.* the simulation lasted long enough for the dislocation to go through the simulation cell over the periodic boundary conditions several times. The large obstacles had three to four unpinnings and the smaller ones upto seven. In these simulations the possible induced features on the dislocations are present during the next unpinnings, which is not equivalent to pristine dislocations interacting with the modified obstacles.

The investigated obstacles were: Cementite- (Fe_3C), amorphous cementite-, $Fe_{23}C_6$-, $Cr_{23}C_6$- and coherent Cr-precipitates, cementite rods, voids, fixed spheres and fixed rods. All obstacles except the cementite rods and fixed rods were spherical, and the rods were cylindrical with the axis perpendicular to the slip plane. The cementite rods were almost as long as the height between the fixed layers and the fixed rods were as high as their diameter. The results for the unpinning stresses for spherical cementite, $Fe_{23}C_6$- and $Cr_{23}C_6$-precipitates and the cementite rods are taken from Refs. 8 and 9. Also some of the unpinning mechanisms are touched in these previous studies. In the simulation of the voids, fixed spheres and coherent chromium precipitates the amount of atoms in the obstacle were 44, 349 and

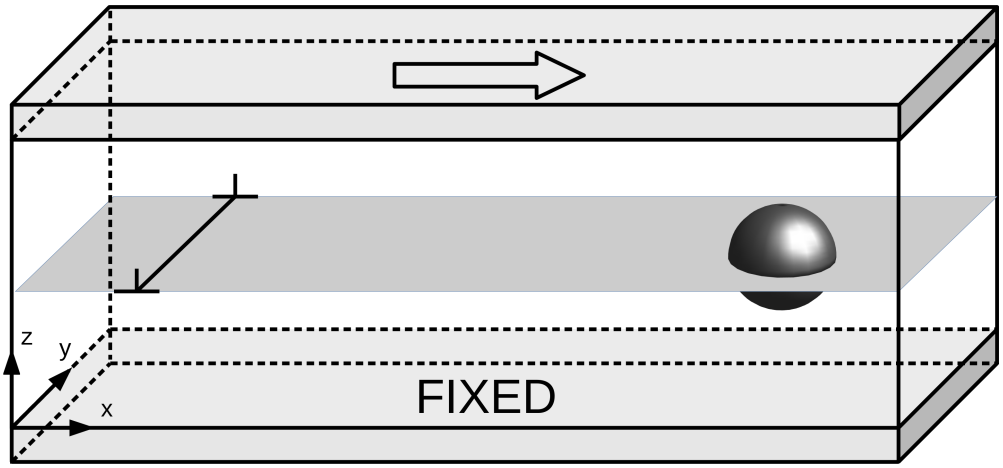

Figure 1. Schematic illustration of the system setup.

2775 vacancy/fixed/chromium atoms for the 1 nm, 2 nm and 4 nm obstacles, respectively. The fixed rods contained 67, 480 and 4042 fixed atoms, respectively. All simulations were conducted with three different initial seeds, to investigate the stochastic part of the unpinning mechanisms. The exceptions were the amorphous cementite, the fixed sphere and fixed rod simulations. For the amorphous cementite simulations three different amorphous structures were investigated, in addition to three different initial seeds for one of the investigated structures. When fixed spheres/rods were investigated the result is the average over several interactions. All the unpinning stresses given in the Results section is the average of the three initial seeds/structures.

3. Results and Discussion

This section is structured as follows; First the unpinning stresses for the obstacles during the first unpinning event is presented; Second the mechanism present during this event is described in more detail; Last the evolution of the obstacle and dislocation is described during multiple interactions, and also the consequences of this.

3.1. Unpinning stress

The unpinning stresses for all obstacles can be seen in Figs. 2, 3 and 4, for the 1 nm, 2 nm and 4 nm obstacles, respectively. These results are the unpinning stress for the first interaction with the obstacle, the evolution of the unpinning stress during multiple interactions are described later, in Section 3.3. The first conclusions that can be seen is that an increasing temperature have a lowering effect on the unpinning stress, which has been seen in many previous studies [11]. Another thing also seen before is that a larger obstacle will yield a higher unpinning stress. The only exception in the used potential is the coherent Cr-precipitates, where these two conclusions are not evident. The difference between the different seeds for the same obstacles showed very small differences. Mainly the difference was seen for the small sizes and at low temperature, where the stochastic movement of atoms that triggers the unpinning is not present as often as at higher temperature [9].

In previous studies it was shown that three different carbides, cementite, $Fe_{23}C_6$ and $Cr_{23}C_6$, of sizes 2 nm and 4 nm showed similar unpinning stresses [9]. There were a larger difference between the 1 nm spherical $Fe_{23}C_6$ compared to the others. The reason for the 1 nm $Fe_{23}C_6$ results can probably be explained by the weaker bonding between Fe-C than Cr-C. As seen in Ref. 9 the cementite rod did have a higher unpinning stress than all of the other carbides, which showed the importance of surface curvature in the unpinning phenomenon.

If the results for the carbides previously studied [9], cementite, $Fe_{23}C_6$ and $Cr_{23}C_6$, are compared with amorphous cementite, we see that the amorphous cementite will agree very well with the previous results. For the 2 nm and 4 nm obstacles we see the same results, and for the 1 nm amorphous cementite obstacles the unpinning stress is a little bit lower than the cementite and $Cr_{23}C_6$ but higher than the $Fe_{23}C_6$. At the two larger sizes the difference between

different amorphous regions did not affect the unpinning stress any more than the difference in stress due to different seeds. For the 1 nm amorphous region the different seeds did not affect the unpinning stress any more than for other obstacles, but the different amorphous regions did drastically affect the results. This shows that some of the small obstacles were more stable than others and this can explain the difference in unpinning stress between the amorpous cementite obstacles and the other carbides. Some of the 1 nm amorphous regions became more like a carbon rich 'volume', with not that different structure from the normal BCC structure.

The results show that the void has about the same pinning strength as the carbides for the 1 nm and 2 nm voids. But for the size of 4 nm, we see a significantly lower unpinning stress for the voids, compared to the 4 nm carbides, about 100 MPa to 200 MPa. The fixed atoms in the two different shapes show the highest unpinning stresses. For the two smaller sizes the spherical fixed atoms show similar results to the rod shaped cementite, but for the 4 nm fixed atoms in a sphere is much stronger than the cementite rod. The cylindrical fixed atoms are much stronger than all the other investigated obstacles, and also stronger than the spherical fixed atoms. The difference between the fixed sphere and fixed cylinder is on average 24%, which is very close to the difference in area of the obstacle seen by the dislocation, this phenomenon will be described in more detail in Section 3.2.

At the first interaction the smaller coherent Cr-precipitates are stronger than the 4 nm Cr-precipitates. All of these unpinning stresses are between 50 MPa and 150 MPa, which are lower than all other obstacles at 1 nm and the 2 nm. At 4 nm the results are much lower than the corresponding unpinning stresses for the other obstacles. The almost inverse size dependence of the chromium precipitates are in contradiction to other studies [12]. This is due to how the potential is describing the Fe-Cr and Cr-Cr interaction. The evolution of the unpinning stress for these obstacles show another feature, which is described in the Section 3.3. Also the unpinning stress was quite small for the first interaction at the higher temperatures and could vary quite a bit between different runs, which make the numerical values only indicative, but the qualitative results are still valid.

The results show that there are 4 different groupings for the unpinning stresses. The fixed obstacles, the hard obstacles, the voids and the coherent obstacles. At the smaller sizes the differences are not as clear as for the larger size, where there is a clear separation for these different obstacles. This suggests that the mechanism is different for each of these groups. This is discussed more in detail in the next section, Section 3.2.

3.2. Unpinning mechanism

In this section we describe the unpinning mechanism for all investigated obstacles during the first interaction. The evolution and consequences of the unpinning mechanism during consequtive unpinnings are described in the next section, Section 3.3.

The coherent chromium precipitates, all sizes and at all temperatures, were sheared at the dislocation plane. This means that the upper part of the obstacle was shifted one Burger's vector per interaction. It was also seen for all sizes that the dislocation was trapped at the interface between the different elements. But when the interface was penetrated the dislocations could easily pass through the chromium volume. For the larger obstacles the interface was apparently less disorted, which can explain that it could be more easily penetrated, and therefore the strength of the large obstacles were lower than for the smaller precipitates. The disortion also played an important role when the dislocation interacted with the same obstacle multiple times, described in Section 3.3. From the results we see that the shear mechanism both depend on the interface strength and the strength of the impurity atoms. In our case we saw that the interface was the strong part whereas the dislocation could easily go through the coherent Cr-region.

For both of the fixed obstacles, spherical and cylindrical, a Hirsch like bypass mechanism [13, 14] was present at all temperatures and sizes. The Hirsch mechanism seen in our investigation is schematically presented in Fig. 5. The dislocation gets trapped around the fixed obstacle and generates screw-dislocation arms that are similar to the Orowan mechanism, described later. After a while one of the screw-dislocation arms will start to go over the obstacle and finally combine with the other screw dislocation of the opposite sign. This will let the edge-dislocation pass the obstacle, but leaving a dislocation loop on the other side on the obstacle and a superjog on the edge-dislocation. The dislocation loop and the superjog on the edge dislocation were during the next passthrough perfectly absorbed, which led to a perfect edge-dislocation, and this was why the same cell could be used to get the statistics. Even though both of the obstacles were bypassed by the same mechanism, there was a difference in the area of the generated loop and superjog. The difference in area between a cylinder and a sphere in the direction the dislocation sees the obstacle is 21.5%, which is very close to the difference in the unpinning stresses between the obstacles, about 24%. This is also the difference in area of the generated loop.

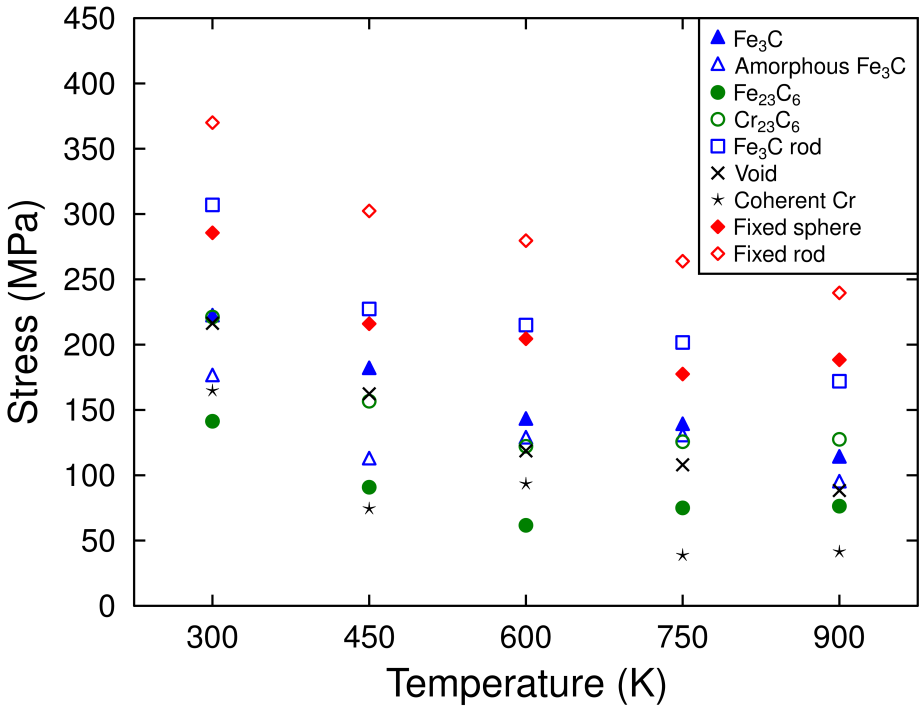

Figure 2. Unpinning stresses for 1 nm obstacles.

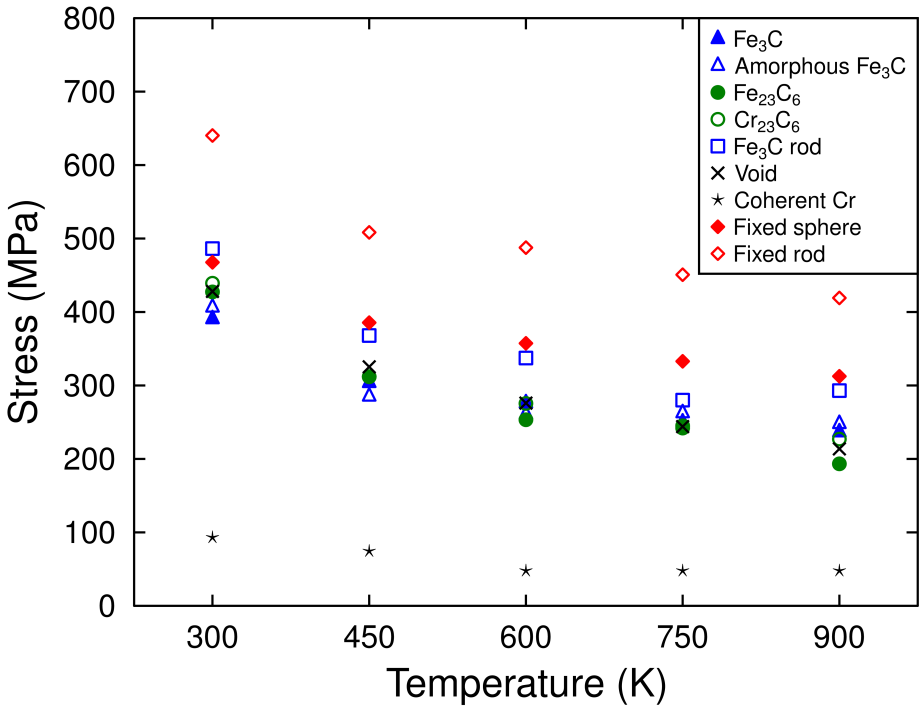

Figure 3. Unpinning stresses for 2 nm obstacles.

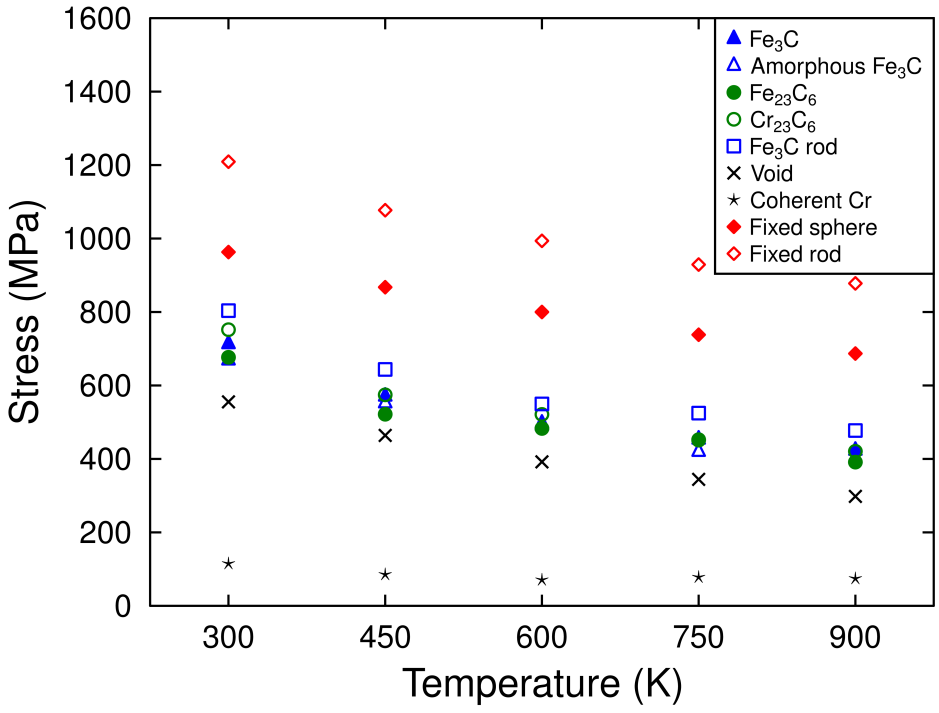

Figure 4. Unpinning stresses for 4 nm obstacles.

In the investigation of the interaction of an edge dislocation with voids, we saw that the dislocation was first attracted to the void. This can be explained by the minimization of the length of the edge-dislocation, which lead to a lower defect energy in total, even if the void was deformed. This absorbtion pins the dislocation, because a new segment of the dislocation must be generated before the dislocation can unpin from the void. Also absorbtion of vacancies was seen during the unpinning, which led to a jog on the unpinned dislocation. This led to a smaller segment of edge-dislocation that had to be generated, which is energetically more favourable. The width of the jog was about the same as the width of the void, also the amount of climb was proportional to the size. The larger the size the more vacancies were absorbed. For the 4 nm void, the amount of absorbed vacancies was increasing with increasing temeperature, for the smaller ones there were no difference.

For all carbides, spherical, rod-shaped and amorphous, there were two different machanisms, depending on size. For all 2 nm and 4 nm obstacles the mechanism was the Orowan mechanism [15]. The dislocation was trapped by the obstacle and with increasing stress a screw-dipole was generated. The absorption of the screw-dipole will eventually let the dislocation unpin. Most of the obstacles were not sheared by the first interaction, even though it was not always clear, especially in the case of the amorphous structure. There was also climb involved in the unpinning phenomenon for these two sizes. Both the screw-dipole could climb along the pricipitate surface as well as vacancies/interstitials were absorbed during the unpinning process, leading to a jog on the unpinned dislocation. Even though the unpinning stress did not drastically change for the different carbides, the sign of climb did change. All three cementite obstacles and the $Cr_{23}C_6$ showed a negative climb, whereas the $Fe_{23}C_6$ showed a positive. This shows the importance of the microstructure and the disortion at the interface between the precipitate and the matrix. The results showed that least climb was seen for the amorphous cementite, whereas the rod showed the most climb. Temperature did not affect the unpinning mechanism, but an increasing temperature will lower the needed unpinning stress. This can be explained by the enhanced screw-dipole absorption at higher temperatures.

For the 1 nm carbides, different mechanism were seen. The cementite precipitate and the rod shaped cementite showed a Orowan(-like) mechanism, even though the obstacles were not strong enough to withstand the loop, and were sheared. The amorphous cementite showed a similar mechanism for some of the structures, so apparently some structures were strong enough for the Orowan(-like) mechanism. The other amorphous cementite obstacles showed a combination of climb and shear, which also was seen for the $Fe_{23}C_6$ precipitate. The $Cr_{23}C_6$ did also show a Orowan(-like) mechanism, but the amount of climb was similar to the $Fe_{23}C_6$. The results showed that the $M_{23}C_6$ precipitates induced much more climb than the spherical cementite and the strong amorphous cementite. Even thoug the cementite rod induced the most climb, there were no gain, which still resulted in a much higher unpinning stress than the other ones. The unpinning stresses for the obstacles with Orowan(-like) mechanism were much higher than the shear/climb combination. Both the $M_{23}C_6$ precipitates showed the same amount of climb, the Cr-precipitate still acted as a much stronger obstacle, due to that the Cr-atoms acted as stronger obstacles than Fe-atoms, in the Fe-matrix.

From the Figs. 3 and 4 we see that the obstacles with the same mechanism, will have a similar unpinning stress. The only exception is the rod, which shows that the climb will drastically affect the unpinning stress [9]. The reason is that the climb will reduce the effective size of the obstacle, so both the generated loop will be smaller and the screw-dipole arms are closer to each other, and this will lower the needed stress. To determine the stress for a certain size, one should use the results for the rod, where the effect of climb is not present. So to be able to determine the exact strength of an obstacle one needs to know the both the mechanism and how the microstructure will introduce other mechanisms, like climb in the case of carbides.

3.3. Multiple interactions with obstacles

In this section we describe the evolution of both the obstacles as well as the dislocation during multiple interactions. The consequences of the interaction mechanism will also be presented.

The fixed atom obstacles, fixed sphere and rod, did not change over time per definition and the generated disloction loops were absorbed by the dislocation creating a perfect edge-dislocation again. This was why the same simulation could be used to get the statistics, because every interaction was the same as the initial interaction. More of the unpinning phenomenon is explained in Section 3.2.

The coherent chromium obstacles were sheared at all temperatures and sizes, which will lead to that after a certain amount of interactions the obstacle will be destroyed. We saw an almost inverse size dependence on the unpinning stress during the first interactions, but during the next interactions we saw that the larger obstacles became much

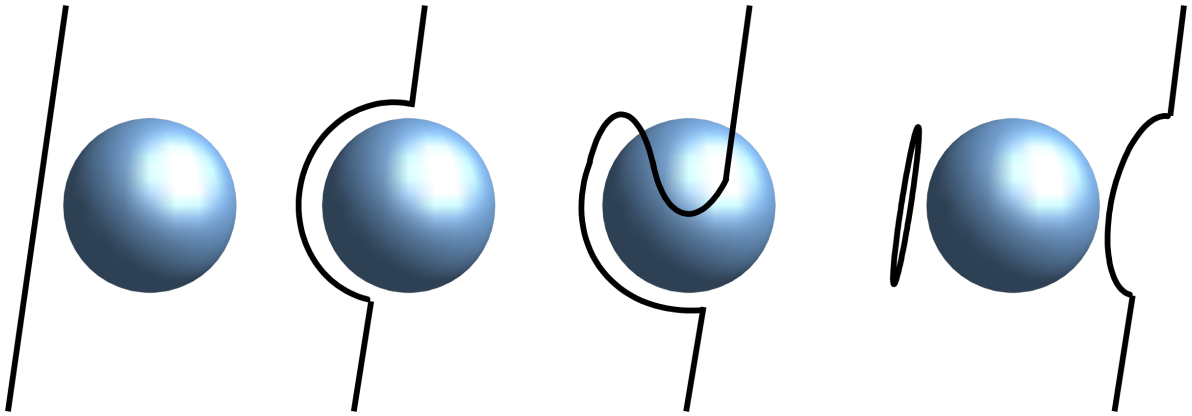

Figure 5. Bypass by Hirsch mechanism

stronger. During the next interactions there is a much larger amount of interface between the Fe- and Cr-atoms, which acts as an obstacle for the dislocation, which leads to a much higher unpinning stress for the large obstacle.

The evolution of the void during several interactions depended on the amount of absorbed vacancies. For the smallest obstacles the amount of absorbed vacancies was enough for the dislocation to pass without interacting with the obstacles during the next interactions, leading to an almost pristine obstacle after several interactions. For the larger voids, the total amount of absorbed vacncies did increase during consequtive interactions, which lead to a larger super jog, eventually large enough to pass without interaction. This also meant that the voids, at least in the beginning, did change its shape at the height where the dislocation interacted with the void. The evolution of the unpinning stress did depend mainly on how the dislocation and void was deformed, and no clear trend could be seen.

All the different carbides did shear after a few interactions, the 1 nm already at the first interaction and the larger after a few interactions. This means that the precipitates did not withstand the force of the generated Orowan loop plus the dislocation. This means that even if the obstacles are stronger than the others investigated, except the fixed atoms, they will be destroyed eventuelly. In most of the cases for the largest obstacle the dislocation absorbed more vacancies/interstitials during consequtive interactions, leading to a smaller effective diameter of the obstacle. For the two smaller obstacles the absorption depended on how exactly the interaction happened, so no clear trend could be seen. For all sizes the carbides were sheared at some height of the obstacle, depending on the super jog magnitude, if the dislocation did not absorb enough vacancies/interstitials to pass without interaction.

The results from multiple interactions with the same obstacles obstacles shows that it is almost impossible to predict exactly what will happen when non-pristine obstacles will interact with dislocation with some induced features, like super jogs. In real materials there will be many different combinations of consequtive interaction of perfect and imperfect dislocations with obstacles, that are preistine and non-pristine.

4. Conclusions

In this Article we have investigated which mechanisms are present during the unpinning of edge-dislocations from diffetent kinds of obstacles. The unpinning stress was also determined, and how it relates to the unpinning mechanism. We studied obstacles of four different natures, for some of them we studied several different types (*e.g.* shape, structure and composition). The effect of size and temperature on all properties was also determined.

We found, as in many previous studies, that for most of the obstacles an increase in temperature will yield a lower unpinning stress and that a larger obstacle will yield a higher unpinning stress. We found that the temperature did not change the unpinning mechanism present, but that size, composition and structure can in some cases change the mechanism.

The four different natures of obstacles each showed a different unpinning mechanism. The coherent obstacles showed a shear mechanism and the voids showed an absorption in the beginning and then a generation of a dislocation segment at the unpinning moment. Both of the fixed obstacles showed a Hirsch-like mechanism, where the magnitude

of the generated superjog and dislocation loop was proportional to the obstacle size, leading to different unpinning stresses. The carbides showed a different mechanism depending on size and composition. For the larger carbides an Orowan mechanism were present for all five kinds. For the smallest ones, a difference could be seen depending on composition and structure, some were strong enough to withstand the Orowan mechansim whereas some were weaker and were sheared by the dislocation.

The results show that as a first approximation the different mechanisms will yield the same unpinning stress. But to understand the full effect and to get the small differences in the unpinning stress the nanostructure must be considered. We have showed that small changes in the composition or structure will in some cases even change the mechanism of unpinning. This will lead to different unpinning stresses as well as a difference in the evolution of both the obstacle and the dislocation. The latter one will change the evolution of the material over a longer time. The shape of the obstacle will both affect the effect of climb as well as increase the amount of obstacle area the dislocation sees. The mircostructure was also seen to change the sign and amount of climb, which will impact the evolution of the material.

Acknowledgments

We would like to thank Krister O. E. Henriksson for the amorphous cementite structures and Dmitry Terentyev for fruitful discussions. This research was funded by the Academy of Finland project SIRDAME (grant no. 259886). We thank the IT Center for Science, CSC, for grants of computational resources. This work has been carried out within the framework of the EUROfusion Consortium and has received funding from the Euratom research and training programme 2014 – 2018 under grant agreement No 633053. The views and opinions expressed herein do not necessarily reflect those of the European Commission.

[1] Y. Xiang, L. T. Cheng, D. J. Srolovitz, W. E, A level set method for dislocation dynamics, ACTA MATERIALIA 51 (18) (2003) 5499–5518.
[2] Y. Xiang, D. J. Srolovitz, L. T. Cheng, W. E, Level set simulations of dislocation-particle bypass mechanisms, ACTA MATERIALIA 52 (7) (2004) 1745–1760.
[3] Y. Xiang, D. J. Srolovitz, Dislocation climb effects on particle bypass mechanisms, PHILOSOPHICAL MAGAZINE 86 (25-26) (2006) 3937–3957.
[4] K. Nordlund, M. Ghaly, R. S. Averback, M. Caturla, T. Diaz de la Rubia, J. Tarus, Defect production in collision cascades in elemental semiconductors and FCC metals, Phys. Rev. B 57 (13) (1998) 7556–7570.
[5] M. Ghaly, K. Nordlund, R. S. Averback, Molecular dynamics investigations of surface damage produced by kiloelectronvolt self-bombardment of solids, Phil. Mag. A 79 (4) (1999) 795.
[6] K. O. E. Henriksson, C. Björkas, K. Nordlund, Atomistic simulations of stainless steels: a many-body potential for the Fe-Cr-C system, Journal of Physics: Condensed Matter 25 (44) (2013) 445401.
[7] Y. N. Osetsky, D. J. Bacon, An atomic-level model for studying the dynamics of edge dislocations in metals, Modelling and Simulation in Materials Science and Engineering 11 (4) (2003) 427.
[8] F. Granberg, D. Terentyev, K. Nordlund, Interaction of dislocations with carbides in BCC Fe studied by molecular dynamics, J. Nucl. Mater. 460 (2015) 23–29.
[9] F. Granberg, D. Terentyev, K. Nordlund, Molecular dynamics investigation of the interaction of dislocations with carbides in BCC Fe, Nucl. Instrum. Methods Phys. Res., Sect. B 352 (2015) 77–80.
[10] A. Stukowski, Visualization and analysis of atomistic simulation data with OVITO the Open Visualization Tool, Modelling and Simulation in Materials Science and Engineering 18 (1) (2010) 015012.
[11] F. Granberg, D. Terentyev, K. O. E. Henriksson, F. Djurabekova, K. Nordlund, Interaction of dislocations with carbides in BCC Fe studied by molecular dynamics, Fusion Sci. Technol. 66 (1) (2014) 283–288.
[12] G. Bonny, D. Terentyev, L. Malerba, Interaction of screw and edge dislocations with chromium precipitates in ferritic iron: An atomistic study, JOURNAL OF NUCLEAR MATERIALS 416 (1-2) (2011) 70–74.
[13] P. B. Hirsch, J. Inst. Metals 86 (1957) 13.
[14] P. B. Hirsch, F. J. Humphreys, in: A. S. Argon (Ed.), Physics of Strength and Plasticity, M.I.T. Press, Cambridge, 1969.
[15] E. Orowan, in: Symposium of Internal Stresses in Metals and Alloys, Inst. of Metals, London, 1948, p. 451.